Waveform inversion for slip distribution of the 2006 Java tsunami earthquake by using 2.5D finite-difference Green's function

Taro Okamoto[1] and Hiroshi Takenaka[2]

[1]*Department of Earth and Planetary Sciences, Tokyo Institute of Technology, 2-12-1 Ookayama, Meguro, Tokyo 152-8551, Japan*
[2]*Department of Earth and Planetary Sciences, Kyushu University, 6-10-1 Hakozaki, Higashi-ku, Fukuoka 812-8581, Japan*

(Received January 30, 2009; Revised March 31, 2009; Accepted April 9, 2009; Online published May 22, 2009)

We first incorporate the large effect of near-source heterogeneity on teleseismic body waveforms in the inversion of the slip distribution of the 2006 Java tsunami earthquake. We incorporate the effect by computing the response of an assumed "2.5D" model structure of the Java trench by a 2.5D finite-difference method. Based on a simulation of inversion, we suggest that intense smearing is possible when we apply 1D Green's functions in the analysis, and that it may obscure the slip pattern. In the inversion of real data, we confirm macroscopic features, such as a long duration (∼165 s) and a slow rupture velocity (∼1.25 km/s). The region of the initial rupture is found to be isolated from the eastern broad region in which we further identify a heterogeneous slip distribution. Most of these regions are likely to be at the sedimentary plate interface where the accreted sediment and the subducting plate are in contact. In particular, the nearly "isolated" feature of a shallow slip region suggests a possible faulting in the shallowest part of the sedimentary plate interface without being strongly enforced by the rupture propagated from the deeper part of the fault. Such heterogeneity suggests a highly variable frictional behavior at the sedimentary plate interface.

Key words: Rupture process, tsunami earthquake, finite-difference method, teleseismic waveform inversion.

1. Introduction

A M_w 7.7 (GCMT) earthquake occurred on July 17, 2006 (USGS PDE: 08:19:26.6, 9.284 S, 107.419 E, depth 20 km) far off the Java Island and generated large, devastating tsunamis: the inundation heights were about 6–7 m along the coast of the Java Island and about 500 persons drowned (Tsuji *et al*., 2006; Kato *et al*., 2007). The event is classified as a "tsunami earthquake" based on surface wave, body wave and tsunami wave analyses (Ammon *et al*., 2006; Fujii and Satake, 2006).

Tsunami earthquakes generate unusually large tsunami waves relative to their surface wave magnitudes (Kanamori, 1972) and are characterized by several common factors, such as long source durations, depletion in high-frequency radiation, and the proximity of their source region to the trench axis (e.g., Pelayo and Wiens, 1992; Polet and Kanamori, 2000; Hara, 2007). Thrust-faulting along the shallow part of the plate boundary is the candidate source of the tsunami earthquake. However, the shallow part of the plate boundary is considered to be a region of low shear strength because of the presence of sediments. Indeed, the transitions in the clay minerals may split the region into an uppermost stable sliding zone and a deeper, stick-slip zone (e.g., Hyndmann *et al*., 1997), and several mechanisms have been proposed to account for faulting at the region (e.g., Tanioka *et al*., 1997; Bilek and Lay, 2002; Seno, 2002). Thus, detailed slip distribution studies would provide important clues in understanding the faulting mechanisms of tsunami earthquakes. Since tsunami earthquakes mark the updip edge of the seismogenic zone, such studies would also provide some insights on seismogenesis at the subduction zone as well as important data towards improving our understanding of the mechanism of tsunami generation (e.g., Tanioka and Seno, 2001).

Teleseismic waveform analysis is one of the most effective methods to estimate slip distribution. However, an analysis of the slip distribution of tsunami earthquakes encounters problems because the strong heterogeneity near the source region causes large effect on the waveforms. The effect, such as large later arrivals, is not reproduced by a one-dimensional (1D) or flat-layered structure that is usually assumed to incorporate the effect of near-source structure (e.g., Wiens, 1989; Okamoto, 1994; Okamoto and Takenaka, in press; see Fig. 1).

We have generated Green's functions for teleseismic body waveforms that incorporate the effect of a "2.5D" crustal model of the Java trench. By using Green's functions for 2.5D and 1D crustal models, we employ a synthetic test to determine the effect of the differences in the Green's functions on the retrieved slip distributions. We then apply the 2.5D Green's functions to invert the real data for the slip distribution of the 2006 Java event.

2. 2.5D Method

We incorporate the effect of the near-source structure by computing the response of a "2D" model (Fig. 1(a)) to an incident plane wave using a 2.5D finite-difference method (Okamoto, 1994; Takenaka and Kennett, 1996). We then convert the response to far-field displacement or the Green's

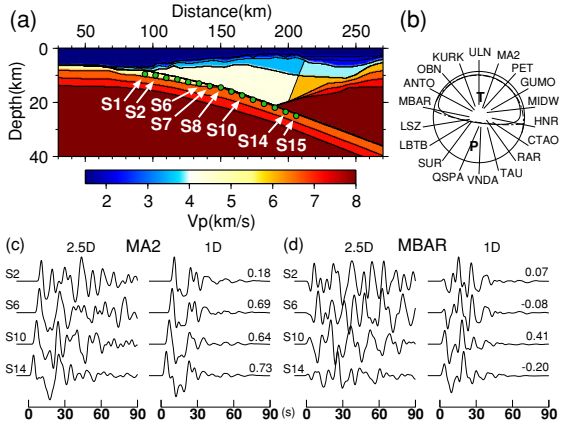

Fig. 1. (a) Cross section of the assumed 2.5D structure. *P*-wave velocity is shown in color scale (*S*-wave velocity is zero in the ocean). Green circles denote the side view of the grid points of the fault plane. There are 15 grid points along the dip and 28 along the strike. The along-dip interval of source points is 8.0 km for the section from S1 to S8 and 8.1 km for the section from S8 to S15. The along-strike interval is 8.2 km. The rigidity for sources S1–S7 is 16.3 GPa and for sources S8–S15, 38.6 GPa. (b) Station coverage plotted onto the Global CMT solution. (c) Examples of synthetic *P*-waveforms (Green's functions) for station MA2. 2.5D denotes those computed for the 2.5D model of the near-source structure, and 1D denotes those for the flat-layered model. Attached indexes (S2–S14) denote the source positions. Numbers attached to the 1D waveforms denote cross-correlation coefficients between 1D and corresponding 2.5D Green's functions for a dulation from 0 to 90 s. The 1D model consists of a standard crust (Kennett and Engdahl, 1991) additionally overlain by a 3-km-thick ocean and 2-km-thick sediment. (d) Same as (c) but for MBAR.

function due to "3D" point source (not 2D line source) buried in the model by applying a reciprocal algorithm. Thus, we call the model a *2.5D model*. The 2.5D model is the same as that used by Okamoto and Takenaka (in press): it is assumed based on the results of seismic surveys in the nearby area (Kopp *et al*., 2002) and global reference models (Dziewonski and Anderson, 1981; Kennett and Engdahl, 1991; Laske *et al*., 2001). With the 2.5D model, the large later arrivals in the waveforms from two aftershocks are well reproduced (Okamoto and Takenaka, in press), which justifies the use of the model.

In our non-linear waveform inversion method, we put point sources with Green's functions $G_{ij}(t)$ at (i, j)-th grid points on the fault and then retrieve the amount of slip (A_{ij}) and onset times (T_{ij}) of them simultaneously. We also retrieve variables B_k that form the shape of the unit source time function (a common shape for all point sources is assumed). The synthetic waveform is:

$$u(t) = \sum_{i,j} A_{ij} \sum_{k}^{N_k} B_k \, G_{ij} \left(t - k\Delta t + T_{ij}\right), \qquad (1)$$

where Δt is the time offset between successive Green's functions that form a unit source time function, and N_k is set to 5. A triangular time function with a basal width of 4 s is used to generate $G_{ij}(t)$ and we assign 2 s for Δt.

We minimize a square residual, R, defined as:

$$R = \left[\mathbf{D}_d \left(\mathbf{u}(\mathbf{x}_A, \mathbf{x}_B, \mathbf{x}_T) - \mathbf{d}\right)\right]^2 + \lambda_A \left[\mathbf{D}_L \left(\mathbf{x}_A - \mathbf{x}_A^{(\ell)}\right)\right]^2 + \lambda_T \left[\mathbf{D}_L \left(\mathbf{x}_T - \mathbf{x}_T^{(\ell)}\right)\right]^2, \qquad (2)$$

where vector $\mathbf{x}_A$ denotes the parameters A_{ij} correctively, $\mathbf{x}_B$ denotes B_k, $\mathbf{x}_T$ denotes T_{ij}, $\mathbf{u}$ the synthetic waveform vector, $\mathbf{d}$ the data vector, and λ_A and λ_T denote smoothing parameters for A_{ij} and T_{ij}, respectively. $\mathbf{D}_d$ is a diagonal matrix whose elements are reciprocals of RMS amplitudes of corresponding waveforms. $\mathbf{D}_L$ is a digital Laplacian operator matrix (Yamanaka and Kikuchi, 2004). We formulate the Hessian matrix based on the standard Levenberg-Marquardt procedure applied to the square residual R (Eq. (2)).

The inversion is non-linear and iterative so we fix the initial vectors $(\mathbf{x}_A^{(\ell)}, \mathbf{x}_B^{(\ell)}, \mathbf{x}_T^{(\ell)})$ through some iterations until a convergence is achieved. We then update all of the initial vectors by assigning the final solutions of the previous inversion, and start a new inversion with the new initial vectors $(\mathbf{x}_A^{(\ell+1)}, \mathbf{x}_B^{(\ell+1)}, \mathbf{x}_T^{(\ell+1)})$. We use uniform initial slip, uniform B_k, and a uniform rupture velocity to generate the first $(\ell = 0)$ initial vectors (note for grids along the edges the initial slip is 1×10^{-4} of that for grids inside the fault, and for corners, it is 1×10^{-8}). We update the initial vectors four times (up to $\ell = 4$) to ensure sufficient final convergence.

We apply a non-negative condition by replacing all of the parameters with squared parameters: e.g., we put $A_{ij} = \alpha_{ij}^2$ and use α_{ij} as the inversion parameters. We re-scale the smoothing parameters when we update the "initial" vectors (including at the first iteration $(\ell = 0)$) because the Jacobian matrix varies with iteration: $\lambda_k (k = A \text{ or } T)$ consists of a constant (fixed up to the final solution) multiplied by the maximum singular value of the Jacobian matrix. (We use the singular value of the Jacobian matrix with respect to the "initial" parameter $\alpha_{ij}^{(\ell)}$.) We set the constants based on the synthetic test so that the solution becomes smooth, yet preserves the input signatures, and fixed them in this paper.

3. Synthetic Test

Based on the 2.5D Green's functions, we make noise-free "synthetic data" (far-field *P*- and *SH*-displacement for the stations shown in Fig. 1(b)) for a time-space slip model (denoted as INPUT in Fig. 2). When we use the 2.5D or correct Green's functions in the inversion (2.5D in Fig. 2), we are able to stably retrieve the positions of the peaks in the slip models. On the other hand, considerable smearing obscures slip patterns when we use 1D Green's functions, which implies a poorer resolution. Thus, it is difficult to separate the slip patches in the shallowest part (about 0–40 km in the DIP direction) and those in the deeper part.

We note that some smearing also occurs in the inversion with 2.5D Green's functions. Nevertheless, the waveforms computed for the retrieved slip pattern reproduce the synthetic data nearly perfectly (traces denoted as 2.5D in Fig. 2). This result demonstrates a practical resolution limit in the teleseismic body waveform inversion: we are unable to discriminate between the assumed (INPUT) and the retrieved (2.5D) slip distributions.

The poor fit of 1D synthetics to data for MBAR may be attributed to the large difference between 1D and 2.5D Green's functions: the cross-correlation coefficients between them for MBAR are quite smaller than those for MA2 (Fig. 1(c, d)). Even with 1D Green's functions, it is possible to improve the fit of the synthetics to the data by adjusting the smoothing parameters and/or the parametrization. How-

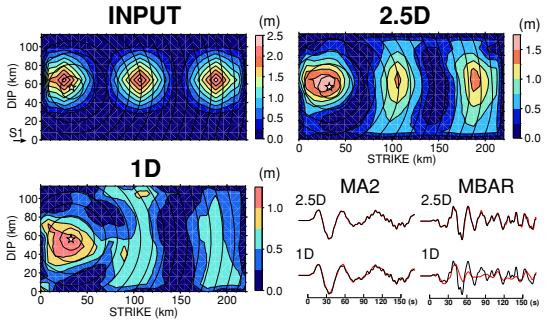

Fig. 2. Results of simulation of inversion. INPUT: assumed slip distribution. 0 km in DIP nearly corresponds to the trench axis (S1 in Fig. 1(a)). Based on the Global CMT solution, dip, slip angles, and strike of the source mechanism are fixed to (10.6, 102.0, 296.0) for grid points in the range from 56 to 113 km in DIP. For shallower points (5.1, 102.0, 296.0) are used. A constant rupture velocity of 1.25 km/s is assumed. 2.5D: inverted slip distribution obtained by using 2.5D synthetics. 1D: inverted slip distribution obtained by using 1D synthetics. Open star denotes the rupture starting point (S8 in Fig. 1(a)). Onset time contours with an interval of 10 s are also shown. In both inversions the same mechanisms as those used for synthetic data are assumed. The color bars are different for each figure. The ratio of the total moment of 2.5D case to that of INPUT model is 1.04, and the ratio of 1D case is 0.89. Right bottom: examples of *P*-waveforms for stations MA2 and MBAR. Black traces are the "synthetic data" and red traces are synthetics reproduced by inversion.

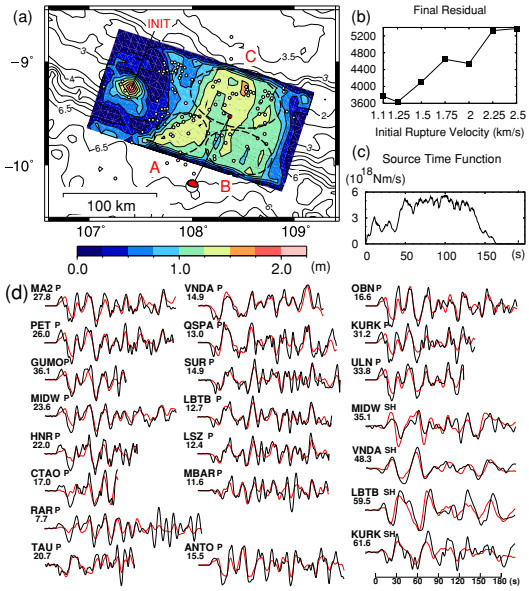

Fig. 3. (a) Inverted slip distribution. The same source mechanisms used in the synthetic test are assumed. "INIT" indicates the rupture starting point (S8 in Fig. 1(a)). Open circles denote the epicenters of 24-h aftershocks (PDE). Global CMT solution of a thrust event (2003/06/01, $M_{\rm w}$ 5.4, depth 15 km) is also shown by a red circle. Bathymetric contour interval is 0.5 km. See text for regions A to C. (b) Dependence of the final residual (Eq. (2)) on the initial rupture velocity. (c) Total source time function. (d) Observed (black) and synthetic (red) waveforms. Attached number denotes maximum amplitude of the observed waveform in μm.

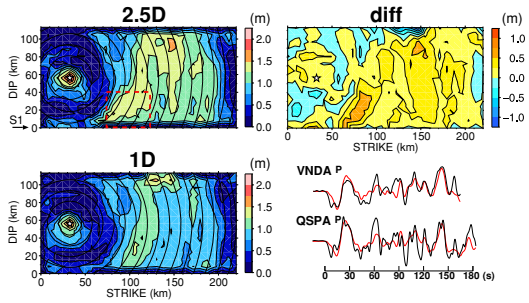

Fig. 4. Slip distributions of the 2006 Java tsunami earthquake by using 2.5D Green's functions (denoted as 2.5D) and 1D Green's functions (1D). Onset times are also shown by black contours with interval of 10 s. Right top (diff) shows the difference between the two slip distributions: slips for 1D case are subtracted from those for the 2.5D case. Right bottom: observed (black) and synthetic (red) waveforms. The synthetics are generated for the same 2.5D slip distribution as shown in left top figure except that the contribution of the slips in the rectangular area (red broken line) is removed.

ever, as apparent in the above results, with incorrect Green's functions, improving the fit does not necessarily guarantee a better solution. It is important to use proper Green's functions to improve the solution.

4. Inversion of Real Data

We collected teleseismic *P*- and *SH*-waveform data of a world-wide broadband network through the IRIS Data Management System. We removed the instrumental response from the raw data and applied a butterworth bandpass filter to obtain components of displacement. The passband for *P*-waves is from 0.005 to 0.2 Hz (0.1 Hz for RAR), and from 0.004 to 0.2 Hz for *SH*-waves.

In the retrieved slip distribution we find a small area of initial rupture with large slips and a broad area of moderate slips in the eastern part of the fault (Fig. 3(a)). The initial rupture area is isolated from the eastern area. We further recognize regions A to C in the eastern area.

It is likely that region A represents an actual slip (i.e., not a result of smearing due to a deeper patch of slips) because there is no deep region with large slips whose onset times coincide with those of region A (from about 40 to 60 s; see Fig. 4(a)). That is, region A is nearly isolated from the deeper part. Slips near the trench axis are also found by tsunami waveform analysis (Fujii and Satake, 2006).

Region B is also in the shallowest part, and some slips (smaller than those in region A) may have also occurred in this region. However, taking the effect of smearing into account (Fig. 2), we can not rule out some smearing that enhanced the retrieved slips in region B because in the deeper part there is an area with large slips (region C). Conversely, region C is likely to represent an actual slip because the synthetic test showed that the positions of the peaks can be retrieved.

We find that a slow rupture velocity is favored (Fig. 3(b): note that Figs. 2–4 are produced for the initial velocity of 1.25 km/s). The favored rupture velocity is lower than the typical value of about 2.5–3.5 km/s for subduction zone earthquakes (Pelayo and Wiens, 1992). We also find a long duration of about 165 s (Fig. 3(c)), which is significantly longer than the typical value of about 30–60 s (Kanamori and Given, 1981). The total seismic moment is estimated to be 5.6×10^{20} N m, which yields a moment magnitude ($M_{\rm w}$) of 7.8: as pointed out by Ammon *et al.* (2006), this is larger than the surface wave magnitude ($M_{\rm s}$) of 7.2. These macroscopic source parameters are consistent with those previously obtained (Ammon *et al.*, 2006; Bilek and Engdhal,

2007) and, together with the proximity to the trench axis (especially that of the region A), they signify that the event was a "tsunami" earthquake.

5. Discussion

Based on the improved resolution, we have found heterogeneous slip distribution: we identified three regions, A to C, in the eastern part of the fault along with the isolated region of initial rupture. Most of these source regions are likely to be at sedimentary plate interface where the accreted sediments and the subducting plate are in contact. This is because, along an survey line near the source region, Kopp *et al*. (2002) found the contact between the accreted materials and the subducting plate extended to about 90 km from the trench axis (see Fig. 1(a) for our model), and most of the high slip regions (except deep part of region C) are within 90 km of the trench axis. In particular, region A might be below the frontal prism as the backstop structure was found about 40 km from the trench axis along the survey line of Kopp *et al*. (2002). Such a heterogeneous slip distribution suggests a spatially variable frictional behavior at the sedimentary plate interface (e.g., Bilek and Lay, 2002): there may be (presumably patchy) regions with unstable frictional behavior at the sedimentary plate interface (i.e., the weak plate boundary). Indeed, a shallow thrust earthquake (M_w 5.4; Fig. 3(a)) occurred as well as the 2006 tsunami event despite the low seismicity in the source region. Also, the nearly "isolated" feature of the shallowest slip region (region A) suggests a possible faulting without being strongly enforced by the rupture propagated from the deeper part of the fault, implying a highly variable frictional behavior at the shallowest part of the sedimentary plate interface.

We have put the rupture starting point near the PDE epicenter. To check the effect of error in the starting point, we supplement the analysis by two inversions, with the starting point being moved trenchward and landward by 16 km (two grids), respectively. The residuals are found to be rather insensitive to the choice of the starting point: a minimum residual is obtained for the case of the point near the PDE epicenter (note the large initial slip moves with starting point).

Finally, we compare solutions for the real data by using 2.5D and 1D Green's functions (Fig. 4: the contribution of region A to the synthetics is also demonstrated). The gross feature (isolated initial slip and eastern moderate slip area) is still observed in the solution by 1D Green's functions. However, slips of 1D case are generally smaller than those of the 2.5D case, especially in region A. We attribute these differences to the degraded resolution in 1D case. Thus, as described in Section 3, with 1D Green's functions it is difficult to discuss the slip distribution in the shallowest part in detail.

Acknowledgments. The non-negative inversion with squared parameters is suggested by Yosihiko Ogata. We are grateful to two anonymous referees for their helpful comments. We used computers at ERI (University of Tokyo). The facilities of the IRIS Data Management System, and specifically the IRIS Data Management Center, were used for access to waveform and metadata required in this study. We used focal parameters available online at NEIC (U.S. Geological Survey), and the Global CMT catalog available at http://www.globalcmt.org. We used the GMT package (Wessel and Smith, 1991). This research was supported by JSPS-KAKENHI (18540418).

References

Ammon, C. J., H. Kanamori, T. Lay, and A. A. Velaso, The 17 July 2006 Java tsunami earthquake, *Geophys. Res. Lett.*, **33**, L24308, doi:10.1029/2006GL028005, 2006.

Bilek, S. L. and E. R. Engdahl, Rupture characterization and aftershock relocations for the 1994 and 2006 tsunami earthquakes in the Java subduction zone, *Geophys. Res. Lett.*, **34**, L20311, doi:10.1029/2007GL031357, 2007.

Bilek, S. L. and T. Lay, Tsunami earthquakes possibly widespread manifestations of frictional conditional stability, *Geophys. Res. Lett.*, **29**, doi:10.1029/2002GL015215, 2002.

Dziewonski, A. M. and D. L. Anderson, Preliminary reference Earth model, *Phys. Earth Planet. Inter.*, **25**, 297–356, 1981.

Fujii, Y. and K. Satake, Source of the July 2006 West Java tsunami estimated from tide gauge records, *Geophys. Res. Lett.*, **33**, L24317, doi:10.1029/2006GL028049, 2006.

Hara, T., Magnitude determination using duration of high frequency energy radiation and displacement amplitude: application to tsunami earthquakes, *Earth Planets Space*, **59**, 561–565, 2007.

Hyndmann, R. D., M. Yamano, and D. A. Oleskevich, The seismogenic zone of subduction thrust faults, *The Island Arc*, **6**, 244–260, 1997.

Kanamori, H., Mechanism of tsunami earthquakes, *Phys. Earth Planet. Inter.*, **6**, 346–359, 1972.

Kanamori, H. and J. W. Given, Use of long-period surface waves for rapid determination of earthquake-source parameters, *Phys. Earth Planet. Inter.*, **27**, 8–31, 1981.

Kato, T., T. Ito, H. Z. Abidin, and Agustan, Preliminary report on crustal deformation surveys and tsunami measurements caused by the July 17, 2006 South off Java Island Earthquake and Tsunami, Indonesia, *Earth Planets Space*, **59**, 1055–1059, 2007.

Kennett, B. L. N. and E. R. Engdahl, Traveltimes for global earthquake location and phase identification, *Geophys. J. Int.*, **105**, 429–465, 1991.

Kopp, H., D. Klaeschen, E. R. Flueh, and J. Bialas, Crustal structure of the Java margin from seismic wide-angle and multichannel reflection data, *J. Geophys. Res.*, **107**, doi:10.1029/2000JB000095, 2002.

Laske, G., G. Masters, and C. Reif, CRUST 2.0: A new global crustal model at 2×2 degrees, http://mahi.ucsd.edu/Gabi/rem.html, 2001.

Pelayo, A. M. and D. A. Wiens, Tsunami earthquakes: slow thrust-faulting events in the accretionary wedge, *J. Geophys. Res.*, **97**, 15321–15337, 1992.

Polet, J. and H. Kanamori, Shallow subduction zone earthquakes and their tsunamigenic potential, *Geophys. J. Int.*, **142**, 684–702, 2002.

Okamoto, T., Teleseismic synthetics obtained from three-dimensional calculations in two-dimensional media, *Geophys. J. Int.*, **118**, 613–622, 1994.

Okamoto, T. and H. Takenaka, Effect of near-source trench structure on teleseismic body waveforms: an application of a 2.5D FDM to the Java trench, in *Advances in Geosciences, Solid Earth Volume*, edited by Kenji Satake, 308 pp (approx.), World Scientific Publishing Company, Singapore, 2009 (in press).

Seno, T., Tsunami earthquakes as transient phenomena, *Geophys. Res. Lett.*, **29**, doi:10.1029/2002GL014868, 2002.

Takenaka, H. and B. L. N. Kennett, A 2.5-D time-domain elastodynamic equation for plane-wave incidence, *Geophys. J. Int.*, **125**, F5–F9, 1996.

Tanioka, Y. and T. Seno, Sediment effect on tsunami generation of the 1896 Sanriku tsunami earthquake, *Geophys. Res. Lett.*, **28**, 3389–3392, 2001.

Tanioka, Y., L. Ruff, and K. Satake, What controls the lateral variation of large earthquake occurrence along the Japan Trench?, *The Island Arc*, **6**, 261–266, 1997.

Tsuji, Y., S. Han, Fachrizal, I. Gunawan, and T. Kato, Distribution of run-up heights of the tsunami of the South off Central Java Earthquake of July, 17, 2006, *Programme and Abstracts, Seism. Soc. Japan, 2006, Fall Meeting*, C002, 2006.

Wessel, P. and W. H. F. Smith, Free software helps map and display data, *EOS Trans. AGU*, **72**, 441, 1991.

Wiens, D. A., Bathymetric effects on body waveforms from shallow subduction zone earthquakes and application to seismic processes in the Kurile Trench, *J. Geophys. Res.*, **94**, 2955–2972, 1989.

Yamanaka, Y. and M. Kikuchi, Asperity map along the subduction zone in northeastern Japan inferred from regional seismic data, *J. Geophys. Res.*, **109**, B07307, doi:10.1029/2003JB002683, 2004.

T. Okamoto (e-mail: okamoto.t.ad@m.titech.ac.jp) and H. Takenaka